

Asymptotical dynamics of askew-polarized spinning top under the radiation reaction torque

Askold Duviryak^{1*}

^{1*}Department for Computer Simulations of Many-Particle Systems, Institute for Condensed Matter Physics of NAS of Ukraine, 1 Svientsitskii Street, Lviv, 79011, Ukraine, <http://orcid.org/0000-0003-0786-4664>.

Corresponding author(s). E-mail(s): duviryak@icmp.lviv.ua;

Abstract

Rotary dynamics of polarized composite particles as dipole rigid bodies is described by the Euler equations singularly perturbed by the radiation reaction torque. The Schott term is accounted, and the reduction procedure lowering higher derivatives is applied. Asymptotic methods of nonlinear mechanics are used to analyze the rotary dynamics of askew-polarized spinning top. Numerical estimates are relevant to the hypothetical DAST-nanocrystals that might possess a huge dipole moment.

Keywords: spinning top, radiation reaction, Schott term

1 Introduction

Nowadays, nanoparticles in optical traps can be spun up to GHz [1, 2]. On the other hand, the dipole moment of some artificially created nanoparticles, such as inorganic nanocrystals CdSe and CdS [3] or cellulose nanocrystals [4] reaches hundreds and thousands Debyes. Under such trends, the effects of radiative spindown may soon become observable experimentally [5], and their theoretical description is timely.

It is shown in [5, 6] that for the description of rotary dynamics of free polarized particles of nanometer size spun up even to GHz the non-relativistic rigid body mechanics combined with the electrodynamics in the dipole approximation is a sufficient theoretical base. Even so, at least two different expressions for the radiation reaction torque acting on a system of constituent charges are known in literature [7, 8]. They are derived in different ways and differ by the term

which is dependent on the third time derivative of the dipole moment of the system. This term is analogous to the Schott term which, in turn, is relevant to the radiation reaction power [9]. Usually, the Schott-like term is neglected and both expressions for the radiation reaction torque are regarded equivalent. Actually, this is not true, as it follows from the discussion about the role of the Schott term in the radiation reaction problem, recently raised in the literature [6, 10, 11].

In the present paper the importance and account of the Schott-like term in the rotary dynamics of dipole composite particles are substantiated. Besides, examples of polarized nanocrystals to which this dynamics may concern are considered.

When regarding the rotary dynamics of a dipole composite particle as a rigid body one arrives at the Euler equations perturbed by the radiation reaction torque. Accounting the Schott term brings higher derivatives into dynamics and

makes the Euler equations singularly perturbed possessing nonphysical solutions. Thus higher derivatives must anyway be removed from the final description of the dynamics. The recipe used in this work and proposed in the previous ones [5, 6] consists in the reduction of higher derivatives by means of the unperturbed Euler equations. The alternative, which is consonant with the traditional viewpoint [7, 8], is a simple neglect of the Schott term, but this may change crucially the evolution of the particle [6].

In [5, 6] the composite particle was modeled as an axially-symmetric spinning top with the dipole moment directed along the symmetry axis. The symmetry in this example simplifies the Euler equations and makes them integrable in both cases: with and without the Schott term. Different dynamics yield different evolutions and predict different far future asymptotical states. The model matches to the aforementioned cellulose nanocrystals possessing 4400 Debyes of the dipole moment [4]. It will be shown that this value may appear insufficient to study experimentally the radiation reaction spindown.

Here we develop the rotary dynamics of the askew-polarized axially-symmetric spinning top. This case is relevant to the hypothetical organic DAST-nanocrystals which are not synthesized yet but predicted to possess millions Debyes of a permanent dipole moment [12]. The axial symmetry in this problem is broken due to incline of the dipole moment. Consequently, the rotary dynamics is described by a complicated nonlinear set of Euler equations which is not integrable. We combine approximation methods such as linearization, asymptotic expansion, averaging and numerical integration in order to study general features and details of the radiative slowdown of the askew-polarized spinning top.

The paper is organized as follows. In the section 2 a balance equation for the angular momentum of a system of radiating charges is considered. Two different expressions for the radiation reaction torque which differ by the time derivative Schott term are discussed, and the corresponding Euler equations describing a rotary motion of a polarized spinning top are presented. The section 3 is devoted to the rotary dynamics of the symmetric spinning top with arbitrarily inclined dipole moment. The Euler equation is split into a coordinate components, and a partial

exact solution is found. In section 4 approximation methods of nonlinear mechanics are used to study the asymptotic behavior of the askew-polarized spinning top. In subsections 4.1–4.4 several asymptotical solutions are found analytically, which are approved by numerical integration in subsection 4.5. In section 5 three special cases of the polarized spinning top are considered – with longitudinal polarization (subsection 5.1), with transverse polarization (subsection 5.2), and the spherical spinning top. The application of aforementioned results to the cellulose nanocrystals and to the hypothetical DAST-nanocrystals is discussed in section 6. The final section 7 includes a summary and conclusions of the paper.

2 Equation of motion of a polarized spinning top

Here we consider a composite particle consisting of point-like charges q with masses m located at positions \mathbf{r} . We proceed from the slow-motion balance equation [7, section 75]:

$$\dot{\mathbf{L}} = \frac{2}{3c^3} \mathfrak{d} \times \ddot{\mathfrak{d}} \quad (2.1)$$

for the angular momentum $\mathbf{L} = \sum m \mathbf{r} \times \mathbf{v}$, where $\mathfrak{d} = \sum q \mathbf{r}$ is the dipole moment of the system, and a summation runs over constituent charges. The expression in r.h.s. is the torque of the Abraham-Lorentz radiation reaction forces acting on constituents of the composite particle. The torque of other forces is supposed to vanish.

This is the case when the composite particle is considered as a rigid body, i.e., a spinning top. A rotational motion of an arbitrary point $\mathbf{r}(t)$ of the top can be presented as follows: $\mathbf{r}(t) = \mathbf{O}(t)\boldsymbol{\rho}$, where $\mathbf{O}(t) \in \text{SO}(3)$ is a rotation matrix, and $\boldsymbol{\rho}$ is a constant position of the point in the proper reference frame of the top. We use a higher derivative rigid body kinematics in eq. (2.1) and arrive at the Euler equation of rotary motion of the spinning top [5, 6]:

$$\begin{aligned} \mathfrak{l}\dot{\boldsymbol{\Omega}} + \boldsymbol{\Omega} \times \mathfrak{l}\boldsymbol{\Omega} = \frac{2}{3c^3} \mathbf{d} \times \{ \mathbf{d} \times (\boldsymbol{\Omega}^2 \boldsymbol{\Omega} - \ddot{\boldsymbol{\Omega}}) \\ + (\mathbf{d} \cdot \dot{\boldsymbol{\Omega}})\boldsymbol{\Omega} + 2(\mathbf{d} \cdot \boldsymbol{\Omega})\dot{\boldsymbol{\Omega}} \}; \end{aligned} \quad (2.2)$$

here $\mathfrak{l} = \|\mathfrak{l}_{ij}\|$ ($i, j = 1, 2, 3$) is the inertia tensor, $\mathbf{d} \equiv \mathbf{O}^T \mathfrak{d} = \sum q \boldsymbol{\rho}$ is a constant dipole moment

of the spinning top in the proper reference frame, the vector $\mathbf{\Omega}$, dual to the skew-symmetric matrix $\mathbf{\Omega} \equiv \mathbf{O}^T \dot{\mathbf{O}}$, is the angular velocity of the spinning top in its proper reference frame, and $\mathbf{\Omega} \equiv |\mathbf{\Omega}|$.

The Euler equation (2.2) contains in its r.-h.s. the 2nd derivative $\ddot{\mathbf{\Omega}}$ multiplied by a small parameter d^2/c^3 , i.e., this equation is a singularly perturbed one, and it possesses redundant solutions which describe non-physical runaway spin up [5]. This difficulty can be avoided by reducing higher-order derivatives in small perturbation terms by usage of the free-motion Euler equation, i.e., the equation of a rotary motion of a free spinning top, and its differential consequence:

$$\dot{\mathbf{\Omega}} = -\mathbf{l}^{-1}(\mathbf{\Omega} \times \mathbf{l}\mathbf{\Omega}), \quad (2.3a)$$

$$\begin{aligned} \ddot{\mathbf{\Omega}} &= -\mathbf{l}^{-1}(\dot{\mathbf{\Omega}} \times \mathbf{l}\mathbf{\Omega} + \mathbf{\Omega} \times \mathbf{l}\dot{\mathbf{\Omega}}) \\ &= \mathbf{l}^{-1}\{(\mathbf{\Omega} \times (\mathbf{\Omega} \times \mathbf{l}\mathbf{\Omega}) \\ &\quad - (\mathbf{l}\mathbf{\Omega}) \times \mathbf{l}^{-1}(\mathbf{\Omega} \times \mathbf{l}\mathbf{\Omega})\}. \end{aligned} \quad (2.3b)$$

General explicit form of the reduced Euler equation is cumbersome and omitted here.

The angular momentum balance equation (2.1) is treated also in another way [7, 8]: the radiation reaction torque in r.-h.s. of (2.1) is recast into two terms:

$$\dot{\mathbf{L}} = -\frac{2}{3c^3} \dot{\mathbf{d}} \times \ddot{\mathbf{d}} \quad (2.4a)$$

$$+ \frac{d}{dt} \frac{2}{3c^3} \mathbf{d} \times \ddot{\mathbf{d}}. \quad (2.4b)$$

The total time derivative term (2.4b) containing the 3rd derivative of the dipole moment $\ddot{\mathbf{d}}$ and referred here to as the Schott-like term [6] is usually regarded as negligibly small if, at least, the system moves quasi-periodically [7, section 75]. Then the use of the rigid body kinematics in the equation (2.4a) leads to the equation

$$\begin{aligned} \mathbf{l}\dot{\mathbf{\Omega}} + \mathbf{\Omega} \times \mathbf{l}\mathbf{\Omega} &= -\frac{2}{3c^3}\{(\mathbf{d} \times \mathbf{\Omega})^2 \mathbf{\Omega} \\ &\quad + (\mathbf{d} \cdot (\mathbf{\Omega} \times \dot{\mathbf{\Omega}}))\mathbf{d}\} \end{aligned} \quad (2.5)$$

which will be referred to as the truncated Euler equation. In contrast to (2.2), this equation is not singularly perturbed, and can be reduced to the normal form without the use of the free-motion Euler equations (2.3).

The neglect of the time derivative term (2.4b) is substantiated by an alternative derivation of the

balance equation in the form (2.4a). It is based on accounting the flux of the angular momentum of the dipole radiation through the sphere embracing constituent charges [7, section 72]. Actually, the result is the hereditary balance equation:

$$\dot{\mathbf{L}}|_t = -\frac{2}{3c^3} \dot{\mathbf{d}} \times \ddot{\mathbf{d}}|_{t-R/c} \quad (2.6)$$

which is the more precise, the larger is the radius R of the sphere. In the limit $R \rightarrow \infty$ it turns into the equations with infinitely retarded time argument. This fact is usually not emphasized, and the balance equation (2.6) might be treated mistakenly as the instantaneous one (2.4a). Dynamical consequences of this confusion will be displayed in next sections.

3 Dynamics of an axially symmetric spinning top with inclined dipole moment

Let us consider the case of the symmetric spinning top with the dipole moment inclined to a symmetry axis by the angle χ . In the properly oriented reference frame, where the ort \mathbf{e}_3 is directed along the symmetry axis of the top, and the dipole moment \mathbf{d} lies in the plane $\text{Oe}_1\mathbf{e}_3$, we have:

$$I_{ij} = I_i \delta_{ij}, \quad I_2 = I_1, \quad 0 < I_3 \leq 2I_1, \quad (3.1)$$

$$\mathbf{d} = \{d_1, 0, d_3\}, \quad d_1 = d \sin \chi,$$

$$d_3 = d \cos \chi, \quad 0 \leq \chi \leq \pi/2 \quad (3.2)$$

(there is no summation over i); see figure 1.

We will consider parameters I_1, I_3, d, χ arbitrary. Then the reduced equation of motion (2.2) splits into the following ones:

$$\dot{\Omega}_1 - \delta \Omega_2 \Omega_3 = -\frac{2d_3}{3I_1 c^2} \{d_3 \Omega_a^2 \Omega_1 - d_1 \Omega_b^2 \Omega_3\}, \quad (3.3)$$

$$\begin{aligned} \dot{\Omega}_2 + \delta \Omega_1 \Omega_3 &= -\frac{2}{3I_1 c^2} \{d_1^2 \Omega_c^2 + d_3^2 \Omega_a^2 \\ &\quad - 3d_1 d_3 \delta \Omega_1 \Omega_3\} \Omega_2, \end{aligned} \quad (3.4)$$

$$\dot{\Omega}_3 = -\frac{2d_1}{3I_3 c^2} \{d_1 \Omega_b^2 \Omega_3 - d_3 \Omega_a^2 \Omega_1\}, \quad (3.5)$$

where

$$\Omega_a^2 \equiv \Omega^2 + \delta(\delta - 2)\Omega_3^2,$$

$$\Omega_b^2 \equiv \Omega^2 + \delta(2\Omega_1^2 - \Omega_2^2),$$

$$\Omega_c^2 \equiv \Omega^2 + \delta(\delta + 1)\Omega_3^2,$$

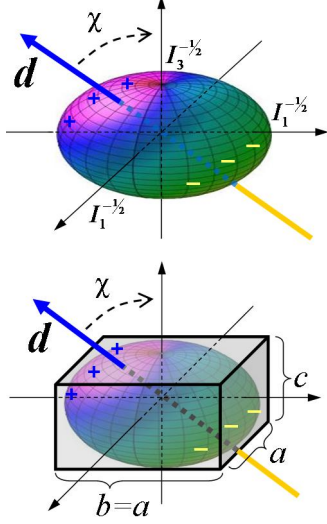
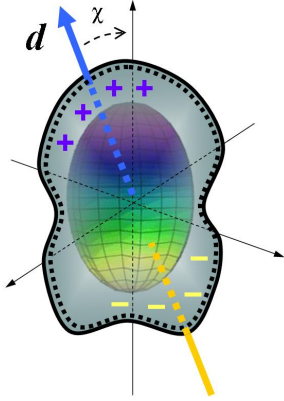


Fig. 1 The model of askew-polarized crystal particle (center). The dipole moment vector \mathbf{d} is inclined to the symmetry axis by the angle χ . The axially-symmetric inertia ellipsoid (i.e., the spheroid) of the crystal (shown inside) is characterized by the principal inertia moments $I_1 = I_2$ and I_3 (top). The model comprises rigid bodies of more irregular shape provided their inertia ellipsoids are axially-symmetric (bottom).



and the parameter

$$\delta \equiv 1 - I_3/I_1, \quad -1 \leq \delta < 1 \quad (3.6)$$

characterizes an elongacy of the inertia spheroid.

One can find easily a particular exact solution corresponding to $\Omega_1 = \Omega_3 = 0$. In this case the equations (3.3) and (3.5) become identities while the equation (3.4) simplifies,

$$\dot{\Omega}_2 = -\tau_0 \Omega_2^3, \quad (3.7)$$

where we introduced the time-scale parameter

$$\tau_0 \equiv \frac{2d^2}{3I_1 c^3}, \quad (3.8)$$

and possesses the particular solution

$$\Omega_2(t) = \Omega_{20}/F(t), \quad \Omega_2(0) = \Omega_{20},$$

$$\text{where } F(t) \equiv \sqrt{1 + 2\tau_0 \Omega_{20}^2 t}. \quad (3.9)$$

It describes a rotary braking of the spinning top which is most intensive during the characteristic time $T = 1/(\tau_0 \Omega_{20}^2)$. Then, at $t \gg T$, the asymptotic regime comes, and the magnitude Ω_2 of the angular velocity ceases by the power law $\Omega_2 \sim \pm 1/\sqrt{2\tau_0 t}$ which does not depend on the initial values. Actually, the partial solution (3.9) coincides with its asymptotics. This becomes evident after redefining the time variable by a finite shift: $t \rightarrow t' = t + T/2$.

General exact solution of the set (3.3)–(3.5) is unknown, thus we apply to approximations.

4 Asymptotical analysis of askew-polarized spinning top dynamics

Let us introduce dimensionless variables:

$$\tau \equiv t/\tau_0, \quad \omega \equiv \tau_0 \Omega, \quad (4.1)$$

where τ_0 is defined in eq. (3.8). In these terms the system (3.3)–(3.5) takes the form:

$$\dot{\omega}_1 - \delta \omega_2 \omega_3 = -n_3^2 \omega_a^2 \omega_1 + n_1 n_3 \omega_b^2 \omega_3, \quad (4.2)$$

$$\dot{\omega}_2 + \delta \omega_1 \omega_3 = -\{n_1^2 \omega_c^2 + n_3^2 \omega_a^2 - 3n_1 n_3 \delta \omega_1 \omega_3\} \omega_2, \quad (4.3)$$

$$(1 - \delta) \dot{\omega}_3 = -n_1^2 \omega_b^2 \omega_3 + n_1 n_3 \omega_a^2 \omega_1, \quad (4.4)$$

where $n_1 \equiv \sin \chi$, $n_3 \equiv \cos \chi$, $0 < \chi < \pi/2$ (in this section) and the dot “ $\dot{\cdot}$ ” denotes differentiation with respect to τ . Combining equations (4.2) and (4.4) yields the equation

$$n_1 \dot{\omega}_1 + n_3 (1 - \delta) \dot{\omega}_3 - n_1 \delta \omega_2 \omega_3 = 0 \quad (4.5)$$

which sometimes is convenient to use, instead of eq. (4.2).

The dimensionless system (4.2)–(4.4) or the equivalent one (4.3)–(4.5) represents two-parametrical family of dynamical systems characterized by the elongacy parameter δ and the inclination angle χ . It is remarkable that the system does not include any small perturbation parameter manifestly. On the other hand, the time scale parameter τ_0 is actually small. Looking ahead let us note that even for strongly polarized DAST-nanocrystal mentioned above $\tau_0 \sim 10^{-27}$ c. Thus, the dimensionless time τ is “fast”, components of the dimensionless angular velocity $\boldsymbol{\omega}$ are small and “slow”, and r.-h.s of the set (4.2)–(4.4) is small compared to separate terms in l.-h.s. This is useful for approximations.

4.1 Power-law monotonous asymptotics

The only fixed point of the system (4.3)–(4.5) is $\boldsymbol{\omega} = 0$. Let us consider an asymptotical behavior of $\boldsymbol{\omega}$ at $\tau \rightarrow \infty$. First of all, we examine the power-law asymptotical behavior and represent the components $\omega_1, \omega_2, \omega_3$ as principal terms of the asymptotic expansion power series,

$$\begin{aligned}\omega_1 &= A\tau^\alpha[1 + O(\tau^{-1})], & \omega_2 &= B\tau^\beta[1 + O(\tau^{-1})], \\ \omega_3 &= C\tau^\gamma[1 + O(\tau^{-1})],\end{aligned}\quad (4.6)$$

similarly to the case of a single nonlinear differential equation [13]. Substituting (4.6) into (4.5) yields the equation:

$$\begin{aligned}n_1\alpha A\tau^{\alpha-1} + n_3(1-\delta)\gamma C\tau^{\gamma-1} - n_1\delta BC\tau^{\beta+\gamma} \\ = O(\tau^{\alpha-2}) + O(\tau^{\gamma-2}) + O(\tau^{\beta+\gamma-1})\end{aligned}\quad (4.7)$$

in which all or at least two leading terms on the l.-h.s. must compensate one another while the remaining term as well as all the right-hand side of eq. (4.7) must be negligibly small compared to the leading terms. The equations (4.3) and (4.4) are treated in similar manner. In such a way we derive the algebraic set of equations for the constants $A, B, C, \alpha, \beta, \gamma$. Since there is not known

in advance which terms are leading and which are minor, one should examine all combinations. As a result, we arrive at two self-consistent possibilities.

The first one,

$$A = C = 0, \quad B = \pm 1/\sqrt{2}, \quad \beta = -1/2, \quad (4.8)$$

restores the exact partial solution (3.9). The second solution, eqs. (4.6) with

$$\begin{aligned}\gamma &= -1/2, \quad \beta = -1, \quad \alpha = -3/2, \\ C &= \pm \sqrt{\frac{1-\delta}{2n_1^2}}, \quad B = -\frac{n_3(1-\delta)}{2n_1\delta}, \\ A &= \frac{B}{\delta C} \{1 - [(1-\delta)^2 + 3n_1^2\delta]C^2\},\end{aligned}\quad (4.9)$$

is not exact but only asymptotical. All components of $\boldsymbol{\omega}$ reveal a monotonous decrease at $\tau \rightarrow \infty$ so that $\omega = |\boldsymbol{\omega}| \sim 1/\sqrt{\tau}$ and $\boldsymbol{\omega} \rightarrow 0$. Amplitudes of this asymptotics are rigidly fixed by parameters of the system. Thus it is plausible that some unique selection or rather narrow set of initial conditions leads to this asymptotics which we will label as the asymptotical solution type “1”. There exist other asymptotical solutions analyzed in next subsections and approved by numerical calculations in subsection 4.5.

4.2 Spiral asymptotics

One should expect that, if $\omega \ll 1$, the dynamical system (4.2)–(4.4) behaves mainly as a weakly perturbed spinning top, i.e., its angular velocity precess around the symmetry axis with slowly varying speed and magnitude. Thus we split the angular velocity vector $\boldsymbol{\omega}$ into longitudinal and transverse components, and the latter present as follows

$$\omega_1 = \omega_\perp \cos \varphi, \quad \omega_2 = \omega_\perp \sin \varphi, \quad (4.10)$$

where the angle φ determines a direction of the transverse vector $\boldsymbol{\omega}_\perp = \{\omega_1, \omega_2, 0\}$, and $\omega_\perp = |\boldsymbol{\omega}_\perp|$. In these terms the equations (4.2)–(4.4) take the form:

$$\begin{aligned}\dot{\omega}_\perp &= -n_3^2\omega_a^2\omega_\perp - \frac{1}{2}n_1^2\omega_c^2\omega_\perp(1 - \cos 2\varphi) + n_1n_3[\omega^2 + 2\delta\omega_\perp^2]\omega_3 \cos \varphi, \\ (1-\delta)\dot{\omega}_3 &= -n_1^2[\omega^2 + \frac{1}{2}\delta\omega_\perp^2(1 + 3\cos 2\varphi)]\omega_3 + n_1n_3\omega_a^2\omega_\perp \cos \varphi, \\ \omega_\perp(\dot{\varphi} + \delta\omega_3) &= -\frac{1}{2}n_1^2\omega_c^2\omega_\perp \sin 2\varphi - n_1n_3[\omega^2 - \delta\omega_\perp^2]\omega_3 \sin \varphi.\end{aligned}\quad (4.11)$$

It follows that components ω_\perp and ω_3 are slow variables while the angle φ is a fast variable. Thus one can apply the averaging method of nonlinear mechanics [14]. Averaging the r.h.s. of the equations (4.11) over the fast variable φ yields the system for the averaged variables $\bar{\omega}_\perp$, $\bar{\omega}_3$, $\bar{\varphi}$:

$$\begin{aligned}\dot{\bar{\omega}}_\perp &= -\{n_3^2[\bar{\omega}_\perp^2 + (1-\delta)^2\bar{\omega}_3^2] \\ &\quad + \frac{1}{2}n_1^2[\bar{\omega}_\perp^2 + (1+\delta+\delta^2)\bar{\omega}_3^2]\}\bar{\omega}_\perp, \\ (1-\delta)\dot{\bar{\omega}}_3 &= -\frac{1}{2}n_1^2[(2+\delta)\bar{\omega}_\perp^2 + 2\bar{\omega}_3^2]\bar{\omega}_3, \\ \dot{\bar{\varphi}} &= -\delta\bar{\omega}_3.\end{aligned}\quad (4.12)$$

This system is exactly solvable as it is similar to that presented in [5, eqs.4.9-11]. But here we are interested in asymptotics.

Again, $\bar{\omega}_\perp$ and $\bar{\omega}_3$ are slow variables while $\bar{\varphi}$ is fast. We put

$$\begin{aligned}\bar{\omega}_\perp &= A\tau^\alpha[1+O(\tau^{-1})], & \bar{\omega}_3 &= B\tau^\beta[1+O(\tau^{-1})], \\ \bar{\varphi} &= C\tau^\gamma[1+O(\tau^{-1})],\end{aligned}\quad (4.13)$$

and substitute into eqs. (4.12). The values of constants $A, B, C, \alpha, \beta, \gamma$ to be found depend on the parameters δ and $\xi \equiv \tan^2\chi$. There are three different cases marked in follows the asymptotics type “1” (in subsection 4.1):

$$2. \quad \alpha = -\frac{(1-\delta^3)}{4} - \frac{(1-\delta)^3}{2\xi} < \beta = -\frac{1}{2}, \quad B^2 = \frac{1-\delta}{2n_1^2} \quad (4.14)$$

$$\text{if} \quad 0 < \xi < 2\frac{(1-\delta)^3}{1+\delta^3}. \quad (4.15)$$

$$3. \quad \alpha = \beta = -\frac{1}{2}, \quad A^2 = \frac{(1+\delta^3)\xi - 2(1-\delta)^3}{\delta n_1^2[2(3-\delta^2) - (3+3\delta+\delta^2)\xi]},$$

$$B^2 = \frac{2(1-\delta) - (1+2\delta)\xi}{\delta n_1^2[2(3-\delta^2) - (3+3\delta+\delta^2)\xi]} \quad (4.16)$$

$$\text{if} \quad \frac{2(1-\delta)^3}{1+\delta^3} \leq \xi \quad \text{and} \quad \xi \leq \frac{2(1-\delta)}{1+2\delta}, \quad \delta > -\frac{1}{2}. \quad (4.17)$$

$$4. \quad \beta = -\frac{(2+\delta)\xi}{2(1-\delta)(\xi+2)} < \alpha = -\frac{1}{2}, \quad A^2 = \frac{1}{2-\xi} \quad (4.18)$$

$$\text{if} \quad \xi > \frac{2(1-\delta)}{1+2\delta}, \quad \delta > -\frac{1}{2}, \quad \text{and} \quad \xi < \frac{4(1-\delta)}{3\delta}, \quad \delta > 0. \quad (4.19)$$

The magnitude A in the case “2” and B in the case “4” remain undetermined within the approximation used. Nevertheless, in all three cases we have $\omega = |\boldsymbol{\omega}| \sim 1/\sqrt{\tau}$ at $\tau \rightarrow \infty$. Domains of the δ - χ parameter plane in which these spiral asymptotical solutions “2-4” exist are outlined in figure 2. In particular, the domain “3” (eq. (4.17)) of the solution (4.13), (4.16) consists of two components conjunct by an isthmus at the point $\delta = 0$, $\chi_0 = \arctan\sqrt{2} = 0.304\pi$.

The averaging of the system (4.11) over the variable φ makes a sense if $\gamma > 0$. This condition violates if

$$\xi > \frac{4(1-\delta)}{3\delta}, \quad \delta > 0. \quad (4.20)$$

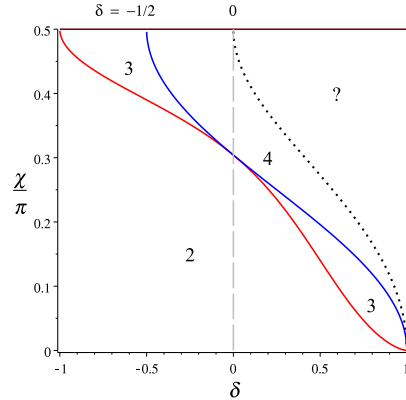


Fig. 2 Domains of the δ - χ parameter plane in which the spiral asymptotical solutions “2-4” exist. In the domain “?” the “fast” variable $\bar{\varphi}$ “stops”: $\bar{\varphi} \sim \tau^\gamma$, $\gamma < 0$, so that the averaging makes no sense.

This means that the assumption about a monotonous decrease of variables ω_\perp , ω_3 and a monotonous increase of φ is not true in the domain (4.20) marked in figure 2 as “?”. Thus one should look in this domain for an asymptotic solution different from spiral ones.

4.3 Oscillating solution on a time segment

Coming back to the exact particular solution (3.9) of the system (3.3)–(3.5) and redefining the time variable t by a finite shift, we have $\Omega_1 = \Omega_3 = 0$, $\Omega_2 = \pm 1/\sqrt{2\tau_0 t}$; see the end of section 3. In terms of dimensionless variables (4.1) this solution reads: $\omega_1 = \omega_3 = 0$, $\omega_2 = \pm 1/\sqrt{2\tau}$. Let us consider a small perturbation to this solution:

$$h \equiv \omega_2 - f, \quad \text{where } f \equiv \pm 1/\sqrt{2\tau} \quad (4.21)$$

and

$$|\omega_1|, |\omega_3|, |h| \ll |f| = 1/\sqrt{2\tau}. \quad (4.22)$$

Introducing a new small variable (instead of ω_1):

$$\omega_\perp \equiv \omega_1 + \frac{n_3}{n_1}(1 - \delta)\omega_3 \quad (4.23)$$

and keeping in eqs. (4.5), (4.4) terms up to linear ones in small variables, one obtains:

$$\dot{\omega}_\perp = \delta f \omega_3, \quad (4.24)$$

$$\dot{\omega}_3 = f^2 \left[\frac{n_1 n_3}{1 - \delta} \omega_\perp - \omega_3 \right]. \quad (4.25)$$

Eliminating ω_3 yields the 2nd-order equation:

$$\ddot{\omega}_\perp + \frac{1}{\tau} \dot{\omega}_\perp \mp \frac{n_1 n_3}{2\sqrt{2}(1 - \delta)} \omega_\perp = 0 \quad (4.26)$$

the solution of which can be expressed in terms of Bessel functions. In order to have a decreasing asymptotics $\omega \rightarrow 0$ at $\tau \rightarrow \infty$, we chose $f(\tau) \equiv -1/\sqrt{2\tau}$ and put $\delta > 0$ (when in the domain “?”, eq. (4.20)). Using, besides, eq. (4.24) one gets:

$$\begin{aligned} \omega_\perp(\tau) &= \frac{4\delta}{\sqrt{2a}} \left\{ A J_0(a\tau^{1/4}) + B N_0(a\tau^{1/4}) \right\}, \\ \omega_3(\tau) &= \tau^{-1/4} \left\{ A J_1(a\tau^{1/4}) + B N_1(a\tau^{1/4}) \right\}, \end{aligned}$$

where $a = 2^{5/4} \sqrt{\frac{n_1 n_3 \delta}{1 - \delta}}$. In asymptotics $\tau \rightarrow 0$

$$\begin{aligned} \omega_1(\tau) &\approx \omega_\perp(\tau) = \frac{4\delta}{\sqrt{2a}} C \tau^{-1/8} \cos(a\tau^{1/4}), \\ \omega_3(\tau) &= C \tau^{-3/8} \sin(a\tau^{1/4}), \end{aligned} \quad (4.27)$$

where A , B and C are arbitrary constants.

Let us consider the correction $h = \omega_2 - f$. Substituting the asymptotics (4.27) into eq. (4.3), keeping leading terms in $1/\tau$ and up to linear terms in the small variable h we arrive at the equation

$$\dot{h} = -\omega_1^2 h - \delta \omega_1 \omega_3 \quad (4.28)$$

which can be solved exactly. Missing details, we represent the asymptotics of the solution:

$$h(\tau) \sim -\frac{a}{2\sqrt{2}\tau^{1/4}} \sin(2a\tau^{1/4}). \quad (4.29)$$

The corrections (4.27) and (4.29) decrease more slowly than the leading term $|\omega_2| = 1/\sqrt{2\tau}$. Thus the approximated solution (4.21), (4.27), (4.29) is not the asymptotics but makes the sense at a finite time segment up to the moment when the conditions (4.22) violate.

4.4 Oscillating asymptotics

The previous oscillating solution on a finite time segment suggests a structure of a possible oscillating asymptotical solution. We suppose that both solutions reveal similar oscillating behavior, but components of the dimensionless angular velocity satisfy asymptotically the relations: $|\omega_1| \sim |\omega_2| \gg |\omega_3|$. Taking these relations into account and using the substitution (4.23) turns the system (4.3)–(4.5) into the exact equation:

$$\dot{\omega}_\perp = \delta \omega_2 \omega_3 \quad (4.30)$$

and the linearized ones:

$$\begin{aligned} \dot{\omega}_2 &\approx -[\omega_\perp^2 + \omega_2^2] \omega_2 - \{\delta - [2(1 - \delta)n_3/n_1 \\ &\quad + 3n_1 n_3 \delta] \omega_2\} \omega_\perp \omega_3, \end{aligned} \quad (4.31)$$

$$\begin{aligned} \dot{\omega}_3 &\approx -\frac{n_1 n_3}{1 - \delta} [\omega_\perp^2 + \omega_2^2] \omega_\perp \\ &\quad - \left[\left(n_1^2 \frac{1 + 2\delta}{1 - \delta} + 3n_3^2 \right) \omega_\perp^2 + \omega_2^2 \right] \omega_3. \end{aligned} \quad (4.32)$$

Then we put:

$$\begin{aligned} \omega_\perp &= f \cos \varphi, & \omega_2 &= g + h, \\ \omega_3 &= v \sin \varphi + w \cos \varphi \end{aligned} \quad (4.33)$$

$$\text{where } f, g \gg h, v, w \quad (4.34)$$

and φ are functions of τ to be found.

Substituting (4.33) into (4.30) and accounting (4.34) to neglect small terms yields the equation:

$$[\dot{f} - \delta gw] \cos \varphi + [f\dot{\varphi} + \delta gv] \sin \varphi = 0$$

which being multiplied by $\cos \varphi$ or $\sin \varphi$ and averaged over φ splits into the pair of equations:

$$\dot{f} = \delta gw, \quad (4.35)$$

$$\dot{\varphi} = -\delta \frac{g}{f} v. \quad (4.36)$$

When treating eq. (4.32) in similar manner one arrives at the following pair of equations:

$$\begin{aligned} \dot{v} &= -\delta \frac{g}{f} wv \\ &- \left[\frac{1}{4} \left(n_1^2 \frac{1+2\delta}{1-\delta} + 3n_3^2 \right) f^2 + g^2 \right] v, \end{aligned} \quad (4.37)$$

$$\begin{aligned} \dot{w} &= \delta \frac{g}{f} v^2 + \frac{n_1 n_3}{1-\delta} \left[\frac{3}{4} f^2 + g^2 \right] f \\ &- \left[\frac{3}{4} \left(n_1^2 \frac{1+2\delta}{1-\delta} + 3n_3^2 \right) f^2 + g^2 \right] w. \end{aligned} \quad (4.38)$$

Defining $g = \bar{\omega}_2$ splits (4.31) into the pair:

$$\dot{g} = - \left[\frac{1}{2} f^2 + g^2 \right] g, \quad (4.39)$$

$$\begin{aligned} \dot{h} &= - \left[f^2 \cos^2 \varphi + 3g^2 \right] h \\ &- \left\{ \delta - \left[2 \frac{n_3}{n_1} (1-\delta) + 3n_1 n_3 \delta \right] g \right\} \times \\ &\times f \cos \varphi \{ v \sin \varphi + w \cos \varphi \}. \end{aligned} \quad (4.40)$$

We look for asymptotical solutions of eqs. (4.35)–(4.39):

$$\begin{aligned} f &= A \tau^\alpha [1 + O(\tau^{-1})], & g &= B \tau^\beta [1 + O(\tau^{-1})], \\ \varphi &= C \tau^\gamma [1 + O(\tau^{-1})], & v &= M \tau^\mu [1 + O(\tau^{-1})], \\ w &= N \tau^\nu [1 + O(\tau^{-1})] \end{aligned} \quad (4.41)$$

and find the following values of parameters:

$$\begin{aligned} \alpha &= \beta = -1/2, & \gamma &= 1/4, \\ \mu &= -3/4, & \nu &= -1, \\ A^2 &= \frac{3(1+\xi)(1-\delta)}{1-\delta-(1-4\delta)\xi}, & B &= -\sqrt{\frac{1-A^2}{2}} \\ C &= -4\delta \frac{B}{A} M, & N &= -\frac{A}{2\delta B}, \\ M^2 &= \frac{n_1 n_3 A^2 [3A^2 + 4B^2]}{4\delta(1-\delta)|B|}, \end{aligned} \quad (4.42)$$

provided

$$\xi > \frac{2(1-\delta)}{7\delta-6}, \quad \delta > 4/7. \quad (4.43)$$

Then we search the asymptotics for h from eq. (4.40) as

$$h \sim K \tau^\varkappa \cos 2\varphi \quad (4.44)$$

and find

$$\varkappa = -1/2, \quad K = A^2/(4B). \quad (4.45)$$

We see that $|h| \ll |g|$ provided $|K| \ll |B|$ which is possible if the first inequality in (4.43) is strong (i.e., “ \gg ” instead of “ $>$ ”).

4.5 Numerical solutions

The asymptotical solutions derived analytically in this section are confirmed by numerical integration of the system (4.3)–(4.5). Of course, numerical solutions can be tabulated in a finite interval of evolution parameter. Nevertheless, a behavior of every numerical solution considered at a large value of τ corresponds to one of asymptotical solutions derived above. Hodographs of typical numerical solutions are presented in figures 3.1–3.5, the monotonous solution “1”, eqs. (4.6), (4.9), exists for arbitrary parameters δ and χ (except $\delta = 0$ and/or $\chi = 0$), and δ – χ domains in which other solutions “2–5” exist are outlined in figure 3.D. It is seen that the domain “5” of the corresponding oscillating asymptotical solution overlaps the domain “?” partially (compare figures 2 and 3.D) but this is a consequence of imperfection of the approximation used. Actually, numerical spiral solutions “4” and oscillating solutions “5” (and also the monotonous ones “1”) coexist in the domains “4”, “?” and “5” of the

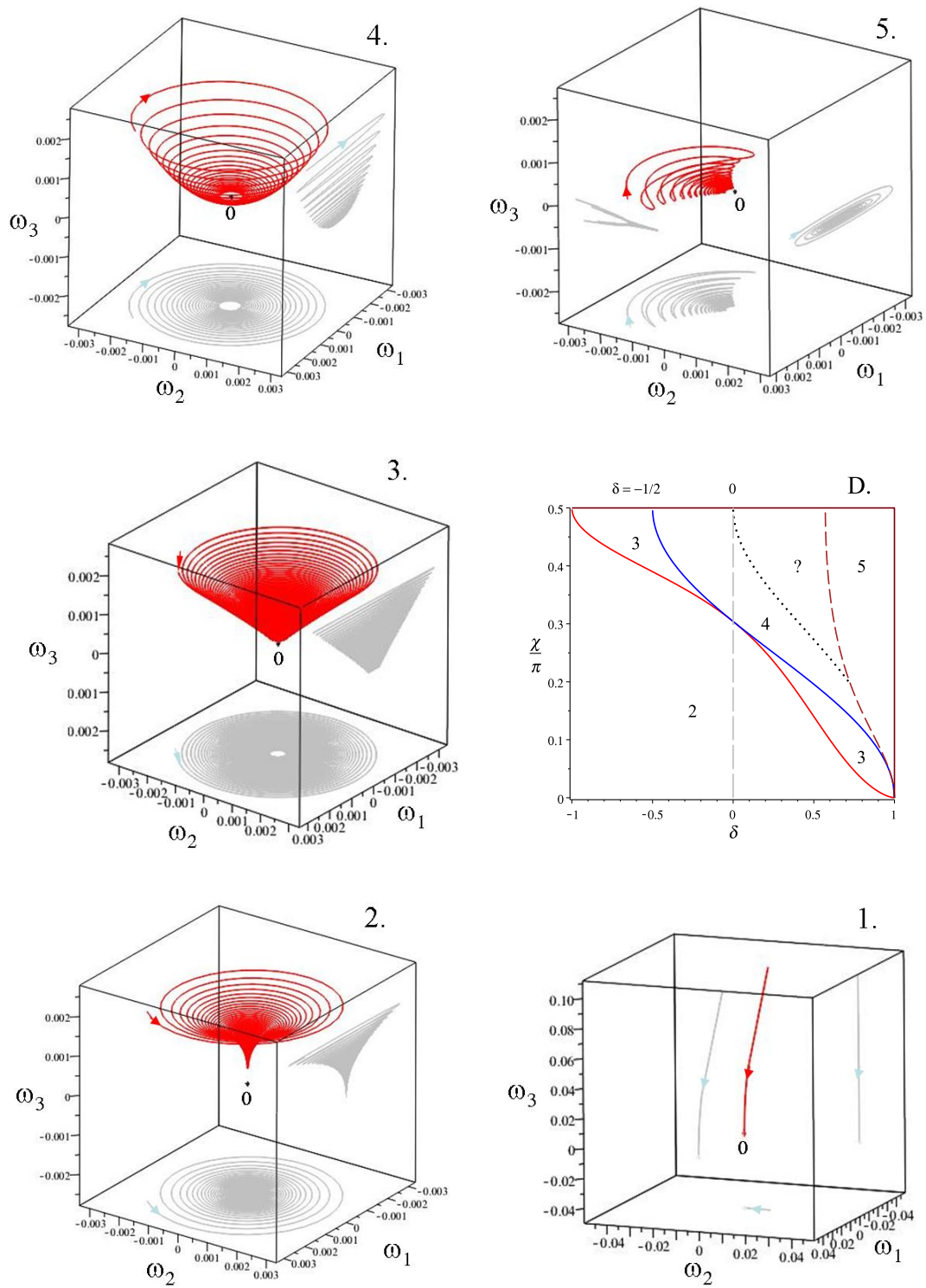


Fig. 3 Hodographs of the dimensionless angular velocity ω of the spinning top following numerical solutions with different asymptotical behavior derived analytically.

parameter diagram 3.D, and a specific evolution of the spinning top in these domains depends on initial conditions.

We recall that aforementioned results are concerned with the cases where a direction of the dipole moment vector does not coincide with any principal axis of inertia. Thus the axial symmetry of the problem is broken.

5 Special cases

Here we consider three special cases where the system possesses a symmetry: L) $\chi = 0$, i.e., $\mathbf{d} \parallel \mathbf{e}_3$, the case of longitudinal polarization; T) $\chi = \pi/2$, i.e., $\mathbf{d} \parallel \mathbf{e}_1$, the case of transversal polarization; O) $\delta = 0$, i.e., $I_1 = I_2 = I_3$, the case of spherical top where the direction of \mathbf{d} alone singles out the symmetry axis of the problem. These cases were partially considered in [5, 6]. Here we outline briefly and complete those results.

5.1 Longitudinal polarization

If $\chi = 0$, i.e., $\mathbf{d} \parallel \mathbf{e}_3$, the problem possesses the axial symmetry. The dimensionless equations of motion (4.2)–(4.4) take the form:

$$\begin{aligned} \dot{\omega}_1 - \delta \omega_2 \omega_3 &= -\omega_1^2 \omega_1, \\ \dot{\omega}_2 + \delta \omega_1 \omega_3 &= -\omega_2^2 \omega_2, \\ (1 - \delta) \dot{\omega}_3 &= 0. \end{aligned} \quad (5.1)$$

In view of the axial symmetry one can put $\omega_1(0) \equiv \omega_{10} = 0$. The set (5.1) possesses the exact general solution:

$$\begin{aligned} \omega_1 &= \omega_{20} \Phi \sin(\delta \omega_3 \tau), & \omega_2 &= \omega_{20} \Phi \cos(\delta \omega_3 \tau), \\ \omega_3 &= \omega_{30} = \text{const}, & \text{where } \Phi &= \sqrt{\frac{\kappa - 1}{\kappa e^{2\epsilon^2 \omega_{20}^2 \tau} - 1}} \\ \kappa &= 1 + \epsilon^2 \frac{\omega_3^2}{\omega_{20}^2}, & \epsilon &= 1 - \delta = \frac{I_3}{I_1}. \end{aligned} \quad (5.2)$$

Thus, $\omega_{\perp} \rightarrow 0$ in the limit $\tau \rightarrow \infty$, and the hodograph of $\boldsymbol{\omega}$ spirales along the plane $\omega_3 = \text{const}$ to the fixed point $\boldsymbol{\omega} \rightarrow \boldsymbol{\omega}_{\infty} = \omega_3 \mathbf{e}_3 \neq 0$ exponentially, by the characteristic time $\Theta = 1/(\tau_0 \Omega_3^2 I_3^2 / I_1^2)$; see figure 4.L.

Quite different evolution of the longitudinally polarized symmetric spinning top follows from the truncated Euler equation (2.5) split by coordinate

components [6] and put here into the dimensionless form:

$$\begin{aligned} \dot{\omega}_1 - \delta \omega_2 \omega_3 &= -\omega_1^2 \omega_1, \\ \dot{\omega}_2 + \delta \omega_1 \omega_3 &= -\omega_2^2 \omega_2, \\ \dot{\omega}_3 &= -\omega_1^2 \omega_3. \end{aligned} \quad (5.3)$$

The solution (corresponding to $\omega_{10} = 0$) [6]

$$\begin{aligned} \omega_1 &= \frac{\omega_{20}}{F} \sin \left\{ \frac{\delta \omega_{30} [F-1]}{\omega_{20}^2} \right\}, \\ \omega_2 &= \frac{\omega_{20}}{F} \cos \left\{ \frac{\delta \omega_{30} [F-1]}{\omega_{20}^2} \right\}, \\ \omega_3 &= \frac{\omega_{30}}{F}, \quad \text{where } F \equiv \sqrt{1 + 2\omega_{20}^2 \tau}, \end{aligned} \quad (5.4)$$

describes the asymptotical power-law spiral decrease of the angular velocity $\boldsymbol{\omega} \sim 1/\sqrt{2\tau} \rightarrow 0$ at $\tau \rightarrow \infty$ along the cone surface, as on figure 3.3. Being natural at the first glance, this solution carries non-physical consequences, as it will be shown in the next section.

The solution (5.2) to the set (5.1) is valid also for the spherical spinning top. In this case $\delta = 0$, the precession of the spinning top is absent, and the spiral hodograph degenerates to the straight line on the plane $\omega_3 = \text{const}$ connecting the initial point $\boldsymbol{\omega}_0$ and the final one $\boldsymbol{\omega}_{\infty} = \omega_3 \mathbf{e}_3$.

Respectively, the hodograph of the solution (5.4) to the set (5.3) reduces at $\delta = 0$ to the straight line connecting $\boldsymbol{\omega}_0$ and $\mathbf{0}$.

5.2 Transversal polarization

In the case $\chi = \pi/2$ the dimensionless equations of motion (4.2)–(4.4) take the form:

$$\begin{aligned} \dot{\omega}_1 - \delta \omega_2 \omega_3 &= 0, \\ \dot{\omega}_2 + \delta \omega_1 \omega_3 &= -\omega_2^2 \omega_2, \\ (1 - \delta) \dot{\omega}_3 &= -\omega_3^2 \omega_3, \end{aligned} \quad (5.5)$$

and an exact solution is still not known. Thus we apply to approximations.

The spiral solutions “3” and “4”, derived for askew-polarized spinning top by the averaging method, are valid in the present case. They reveal the cone-shape trajectories (figure 3.3) if $-1 \geq \delta \geq -1/2$, and the bowl-shape trajectories (figure 3.4) if $-1/2 < \delta < 0$. For the prolate spinning top $\delta > 0$ we should apply to the oscillating solution

“5”, but it does not exist in the case $\chi = \pi/2$. Indeed, since $n_3 = 0$, the magnitude $M = 0$, and then $C = 0$, as it follows from (4.42). Hence the phase variable φ “stops”: $\varphi = 0$, and the averaging method is not applicable in this case. Thus the behavior of the prolate transversally polarized spinning top needs more study.

In contrast to the general case, in the case $\chi = \pi/2$ the dipole vector \mathbf{d} can be directed along the inertia axis $0\mathbf{e}_1$ which is the rotation symmetry axis of order 2. Thus the system of equations (5.3) possesses the set of fixed points $\omega_\infty \mathbf{e}_1$, $\omega_\infty \in \mathbb{R}$ covering this inertia axis. Given ω_∞ , one can linearize the system (5.5) in the vicinity $\omega_1 \approx \omega_\infty$, $|\omega_2|, |\omega_3| \ll |\omega_\infty|$ of the fixed point $\omega_\infty = \omega_\infty \mathbf{e}_1$:

$$\begin{aligned}\dot{\omega}_1 &= 0, \\ \dot{\omega}_2 &= -\omega_\infty^2 \omega_2 - \delta \omega_\infty \omega_3, \\ \dot{\omega}_3 &= -\frac{1+2\delta}{1-\delta} \omega_\infty^2 \omega_3.\end{aligned}\quad (5.6)$$

A search of exponential solutions $\omega - \omega_\infty \mathbf{e}_1 \sim e^{\lambda\tau}$ leads to the characteristic numbers

$$\lambda_1 = 0, \quad \lambda_2 = -\omega_\infty^2, \quad \lambda_3 = -\frac{1+2\delta}{1-\delta} \omega_\infty^2$$

and to the corresponding solution of Cauchy problem

$$\begin{aligned}\omega_1 &= \omega_\infty, \\ \omega_2 &= \omega_{20} e^{\lambda_2 \tau} + \frac{1-\delta}{3} \frac{\omega_{30}}{\omega_\infty} (e^{\lambda_3 \tau} - e^{\lambda_2 \tau}), \\ \omega_3 &= \omega_{30} e^{\lambda_3 \tau}.\end{aligned}\quad (5.7)$$

This solution is stable, i.e., $\omega_2 \rightarrow 0$, $\omega_3 \rightarrow 0$, provided $\lambda_3 < 0$. The latter condition holds for $-1/2 < \delta < 1$. In the domain $-1/2 < \delta < 0$ the solution (5.7) overlaps with the spiral asymptotical solution “4”. Thus two scenarios are possible: the system reaches exponentially the non-zero fixed point $\omega_\infty = \omega_\infty \mathbf{e}_1$, if the initial value $|\omega_\perp(0)| \ll \omega_\infty$, or the spinning top slows down to stop by the power law $\omega \sim 1/\sqrt{\tau} \rightarrow 0$. Both scenarios are approved by numerical calculations [6]; compare figures 3.4 and 4.T.

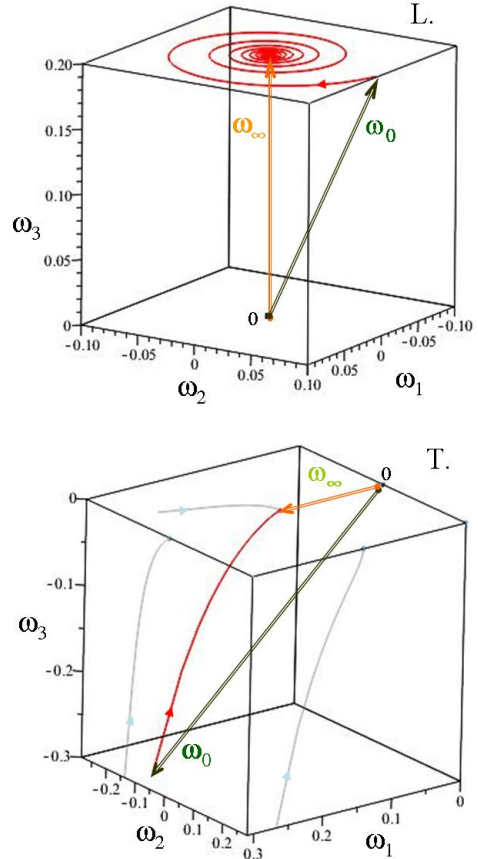


Fig. 4 The spinning top in special cases. L. Longitudinal polarization: exact solution. T. Transversal polarization: numerical solution. In both cases the dimensionless angular velocity tends asymptotically to its residual value ω_∞ directed along the dipole vector \mathbf{d} .

6 Two examples

6.1 The cellulose nanocrystal

The example of an axially-symmetric composite particle with a large longitudinal dipole moment is a cellulose nanocrystal of the slender rod shape with the following characteristics: length $L = 315$ nm, its ratio to diameter $L/D = 10$, density $\rho = 1.6$ g/cm³. The dipole moment $d = 4400$ Debye is directed along a symmetry axis [4]. Thus the relevant to this case solution of the reduced Euler equations is given by eqs. (5.2). It can be easily expressed in terms of the original dimensional variables by means of the relations (4.1).

Approximating the nanocrystal shape by an elongated cylinder yields the following principal inertia moments: $I_1 = 3.3 \cdot 10^{-26}$ g·cm², $I_3 =$

$4.11 \cdot 10^{-28} \text{ g}\cdot\text{cm}^2$. Consequently, the characteristic time scale parameter (3.8) is $\tau_0 = 1.4 \cdot 10^{-35} \text{ c}$, and the ratio $\epsilon = I_3/I_1 = 0.015$ is a small parameter. Given the value of $\Omega_3 = \Omega_{30}$ even record, $\Omega_3 \sim \pi \cdot 10^{10} \text{ c}^{-1}$, the exponential drift $\Omega_{\perp} \rightarrow 0$ is very slow, with the astronomical braking time $\Theta = 1/(\epsilon^2 \tau_0 \Omega_3^2) \sim 10^{10}$ years. Thus, this asymptotical regime is unattainable and can be pushed to infinity by taking the limit $\epsilon \rightarrow 0$ in the solution (5.2), (4.1):

$$\begin{aligned} \Omega_1 &\xrightarrow{\epsilon \rightarrow 0} \frac{\Omega_{20}}{F(t)} \sin(\Omega_3 t), & \Omega_2 &\xrightarrow{\epsilon \rightarrow 0} \frac{\Omega_{20}}{F(t)} \cos(\Omega_3 t), \\ \Omega_3 &= \Omega_{30}, \end{aligned} \quad (6.1)$$

where the square root function $F(t)$ is defined by (3.9). This power-law decrease of $\Omega_{\perp} \rightarrow 0$ is most intensive during the time $T = 1/(\tau_0 \Omega_{20}^2) \sim 3 \cdot 10^6$ years which, although not astronomical, is nevertheless geological, i.e., too large for laboratory observations.

Following the truncated Euler equations (5.3), the limit $\epsilon \rightarrow 0$ of the corresponding solution (5.4) is similarly power-law

$$\begin{aligned} \Omega_1 &\xrightarrow{\epsilon \rightarrow 0} \frac{\Omega_{20}}{F(t)} \sin \Omega_{30} \vartheta(t), \\ \Omega_2 &\xrightarrow{\epsilon \rightarrow 0} \frac{\Omega_{20}}{F(t)} \cos \Omega_{30} \vartheta(t), & \Omega_3 &\xrightarrow{\epsilon \rightarrow 0} \frac{\Omega_{30}}{F(t)}, \end{aligned} \quad (6.2)$$

$$\text{where } \vartheta(t) \equiv \frac{F(t) - 1}{\tau_0 \Omega_{20}^2}, \quad (6.3)$$

but here all three components of the angular velocity decrease with the same geological characteristic time $T = 1/(\tau_0 \Omega_{20}^2) \sim 3 \cdot 10^6$ years.

Actually, the difference between the solutions (6.1) and (6.2) is minor. This is seen better by studying a motion of the nanocrystal in space.

To have a complete description of the rotary dynamics of the rigid body in space, the Euler equations should be complemented by the Poisson equations relating the components of the angular velocity $\Omega = \{\Omega_1, \Omega_2, \Omega_3\}$ as functions of t with the Euler angles φ, θ, ψ and their time derivatives. This set of differential equations has the following normal form [6]:

$$\begin{aligned} \dot{\varphi} &= (\Omega_1 \sin \psi + \Omega_2 \cos \psi) / \sin \theta, \\ \dot{\theta} &= \Omega_1 \cos \psi - \Omega_2 \sin \psi, \\ \dot{\psi} &= \Omega_3 - (\Omega_1 \sin \psi + \Omega_2 \cos \psi) \cot \theta. \end{aligned} \quad (6.4)$$

Since all initial orientations of the free rigid body in an isotropic space are physically equivalent, it is sufficient to find any partial solution of the equations (6.4). Substituting (6.1) into (6.4) yields the exact solution:

$$\varphi(t) = \Omega_{20} \vartheta(t), \quad \theta = \frac{\pi}{2}, \quad \psi(t) = \Omega_3 t. \quad (6.5)$$

It describes a composition of the slowing flat-wise rotation of the cellulose rod and its uniform proper rotation around the symmetry axis with the constant angular velocity Ω_3 .

The functions (6.2)–(6.3) yield a similar to (6.5) solution of the Poisson equations:

$$\varphi(t) = \Omega_{20} \vartheta(t), \quad \theta = \frac{\pi}{2}, \quad \psi(t) = \Omega_{30} \vartheta(t), \quad (6.6)$$

with that difference the proper rotation is not uniform. But the rotation of the rod around its symmetry axis is hardly observable in the $D/L \rightarrow 0$ limit of an infinitely thin rod.

In all respects the cellulose nanocrystals possessing even enormous dipole moment looks to be poor objects for the experimental verification of the radiative spindown.

6.2 The organic DAST-nanocrystal

The example of the permanently askew-polarized composite particle might be the hypothetical organic polar monocrystal of 4-dimethylamino-N-methyl-4-stilbazolium tosylate (DAST), chemical formula $\text{C}_{23}\text{H}_{26}\text{N}_2\text{SO}_3$, which is not synthesized yet but its properties are predicted in literature; see [12] and refs. therein. Crystallographic axes are almost orthogonal thus, if a monocrystal is naturally confined by crystallographic planes, its natural form is a parallelepiped. The dipole moment of a single ion pair is 30 Debyes, it lies in the plane $0e_1e_3$ and is inclined to the axis $0e_1$ by the angle 35° . Taking into account the lattice parameters of such crystal: the cell volume $v = 1.04 \text{ nm} \times 1.13 \text{ nm} \times 1.79 \text{ nm} = 2.1 \text{ nm}^3$, the molecular weigh $\mu = 410.5$, the number of molecules per cell $Z = 4$, one can calculate the density $\rho = 1.37 \text{ g/cm}^3$ and then the principal inertia moments of the nanocrystal. Moreover, the dipole moment of DAST-nanocrystals is predicted to behave as an additive vector characteristic. Thus one can imagine the DAST-nanocrystal of

an arbitrary dimension and a shape, and calculate its inertia tensor and the dipole moment vector.

We are interested in axially-symmetric nanocrystals. Two families are possible.

The first family consists of monocystals of the dimension $a = b \neq c$ with the dipole moment inclined to the symmetry axis $0e_3$ by the angle $\chi = 55^\circ$. The rate of sides c/a determines the rate I_3/I_1 of the principal inertia moments $I_1 = I_2 \neq I_3$, and thus the elongacy parameter $\delta = 1 - I_3/I_1 = (c^2 - a^2)/(c^2 + a^2)$. The DAST-nanocrystal of the dimensions $a = b = 100$ nm, $c = 50$ nm with inertia moments $I_1 = I_2 = 7.14 \cdot 10^{-27}$ g·cm², $I_3/I_1 = 1.6$ (so that $\delta = -0.6$) may possess a huge dipole moment $d = 2.8 \cdot 10^7$ D [12]. Varying the dimensions $a = b$ and c changes the inertia moments I_1, I_3 and the total dipole moment d but keeps unchanged the inclination angle $\chi = 55^\circ$. Thus the only free dimensionless parameter determining the dynamical system remains, i.e., the inertial characteristic δ .

The line corresponding to the 1st family of DAST-monocrystals on the δ - χ diagram (figure 5) crosses the domain “3” close to its isthmus at $\delta = 0$, $\chi_0 = 0.304\pi = 54.7^\circ \approx 55^\circ$, thus the corresponding solution does not apply to this family.

The second family of axially-symmetric DAST-monocrystals corresponds to the dimensions $b = c \neq a$ with the dipole moment inclined to the symmetry axis $0e_1$ by the angle 35° . This family admits all types of solutions presented on figure 3.

Special interest should be paid to the cubic DAST-monocrystals which are equivalent, by inertial properties, to the spherical spinning top. In despite the dipole moment is still inclined to crystallographic axes, the principal inertia axes can be oriented arbitrarily. Choosing $0e_3 \parallel \mathbf{d}$ reduces the dynamical problem to the solvable $\delta = 0$ case considered at the end of subsection 5.1.

Substituting $\delta = 0$ and, consequently, $\epsilon = 1$ into eqs. (5.2), (4.1) yields the following solution of the reduced Euler equations:

$$\begin{aligned} \Omega_1 &= 0, & \Omega_2 &= \Omega_{20} |\Omega_3| \left(\Omega_0^2 e^{2\tau_0 \Omega_3^2 t} - \Omega_{20}^2 \right)^{-1/2}, \\ \Omega_3 &= \Omega_{30}. \end{aligned} \quad (6.7)$$

The corresponding exact solution of the Poisson equations (6.4) is unknown. One can find the asymptotic dependency of the Euler angles on

time:

$$\psi \sim 0, \quad \theta(t) \sim e^{-\tau_0 \Omega_3^2 t}, \quad \varphi(t) \sim \Omega_3 t. \quad (6.8)$$

Hence, at $t \rightarrow \infty$, the DAST crystal rotates around the vertical axis with the angular velocity $\sim \Omega_3$ in such a way that the dipole vector \mathbf{d} spirales to this axis exponentially, with the characteristic time $\Theta = 1/(\tau_0 \Omega_3^2)$.

The solution of the truncated Euler equations follows from eqs. (5.4):

$$\Omega_1 = 0, \quad \Omega_2 = \frac{\Omega_{20}}{F(t)}, \quad \Omega_3 = \frac{\Omega_{30}}{F(t)}, \quad (6.9)$$

and the corresponding exact solution of the Poisson equations (6.4) is:

$$\psi = 0, \quad \theta = \arctan \left| \frac{\Omega_{20}}{\Omega_{30}} \right|, \quad \varphi(t) = \text{sign} \Omega_3 \Omega_0 \vartheta(t); \quad (6.10)$$

here the power-law functions $F(t)$ and $\vartheta(t)$ are defined in (3.9) and (6.3), respectively. This solution predicts the slowing rotation of the crystal to stop around the vertical axis with the dipole vector \mathbf{d} inclined to this axis by the constant angle θ .

For the cubic DAST-nanocrystal of the dimension $a = 100$ nm with equal inertia moments $I = 2.3 \cdot 10^{-26}$ g·cm² and the dipole moment $d = 5.6 \cdot 10^7$ D we have the time scale $\tau_0 = 3.4 \cdot 10^{-27}$ c. Thus, if the initial angular velocity $\Omega_{30} \sim \Omega_{20} \sim \Omega_0 \sim \pi \cdot 10^{10}$ Hz, as in the experiment [2], the characteristic braking time $\Theta \sim 1/(\tau_0 \Omega_0^2) \sim 4$ days which is of order of a storage time in Penning trap [15]. Then such a nanocrystal might serve as a test for choosing between the reduced Euler equation, and the truncated one, that is between the balance equations (2.1) and (2.4a).

7 Conclusions

In the previous paper [5] the equation of rotary motion of a rigid body with the permanent electric dipole moment (2.2) was derived from the Landau-Lifshitz angular momentum balance condition [7, section 75]. This singularly perturbed equation of the 2nd order with respect to the angular velocity $\mathbf{\Omega}$ is then reduced to the 1st-order regularly perturbed equation by means of the unperturbed

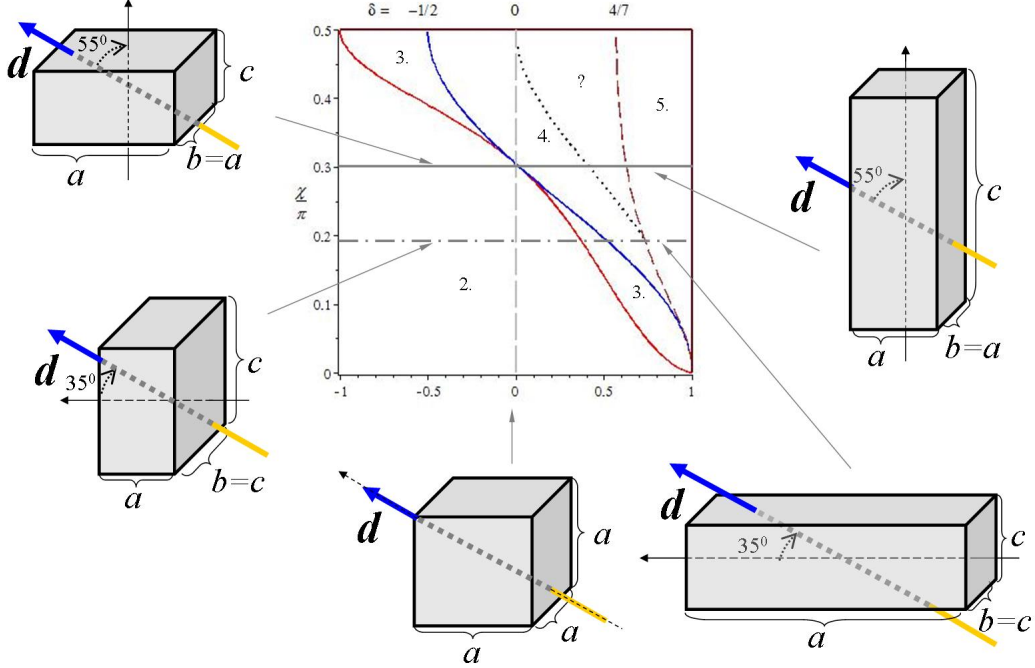


Fig. 5 Two families of axially-symmetric DAST-monocrystals. The 1st family consists of monocrystals of the dimensions $a = b \neq c$ with the dipole moment \mathbf{d} inclined to the symmetry axis $0\mathbf{e}_3$ by the angle $55^\circ = 0.306\pi$ (the solid gray line in the δ - χ diagram). The 2nd family corresponds to the dimensions $a \neq b = c$ with the dipole moment inclined to the symmetry axis $0\mathbf{e}_1$ by the angle $35^\circ = 0.194\pi$ (the dash-dotted gray line). In the $\delta = 0$ case of cubic crystals one of principal inertia axes can be directed along \mathbf{d} .

Euler equation and its differential consequence (2.3).

Another common way to get rid of higher derivatives is to abandon the Schott-type term in the expression for the the radiation reaction torque. It leads to the truncated Euler equation, the correctness of which raises doubts [6].

Here the the case of askew-polarized spinning top with axially-symmetric inertia ellipsoid is considered. This case is suggested by the theoretical works predicted a giant dipole moment of the DAST-nanocrystal; see [12] and refs. therein. The dipole moment vector which is inclined to the symmetry axis spoils the axial symmetry of the problem and complicates the dynamics, when compared to the symmetric case [5, 6].

In general case of inclined dipole moment by the angle $0 < \chi < \pi/2$ a general exact solution of the reduced Euler-type equations (3.3)–(3.5) is unknown. The only partial exact solution (3.9) has been found. Actually, it reveals some general features of the spinning top evolution studied analytically and numerically. Given the initial velocity $\Omega_0 = |\Omega(0)|$, the spinning top slows its

rotation down most intensively during the characteristic time $T \sim 1/(\tau_0\Omega_0^2)$. Then the top gradually switches up to the asymptotic regime in which, at $t \gg T$, the magnitude Ω of the angular velocity decreases by the power law $\Omega \sim 1/\sqrt{\tau_0 t}$, independently on the initial values.

Details of the asymptotical evolution depend mainly on parameters of the polarized spinning top, its elongacy δ and the inclination angle χ , and less on initial data.

First of all we recast the equations of motion in the dimensionless form (4.2)–(4.5) and used asymptotic expansions to examine a monotonous power-law behavior (4.6) of the angular velocity components at $\tau \rightarrow \infty$. We arrive at the asymptotic solution (4.6), (4.9). Numerical calculations show that this asymptotics is inherent to a rather narrow set of initial data.

Then, regarding the radiation reaction torque as a small perturbation (what is actually true), we considered the precessing rotation of the symmetric top and studied its secular evolution using the averaging method.

The averaging method appears not applicable at some values of parameters δ and χ (the domain “?” in figure 2), thus we considered the perturbation of the exact solution (3.9). This perturbed solution makes a sense on the finite time interval, but it has been extended up to a time infinity by the combination of the asymptotic expansion, the averaging and the linearization methods.

As a result, we found five general types of the askew-polarized spinning top evolution which differ essentially from one another but reveal the common asymptotical power law $\Omega \sim 1/\sqrt{\tau_0 t}$ of a spin down.

The monotonous solution “1” describes a decelerating rotation mainly around the symmetry axis $0\mathbf{e}_3$ with quickly ceasing rotations in other directions. This solution is possible for any parameters $-1 < \delta < 1$, $0 < \chi < \pi/2$ if the hodograph of angular velocity passes sufficiently close to the point determined by eqs. (4.6), (4.9) in some instant t . Otherwise, the top undergoes a slowly varying precession. Respectively, the hodograph spirals to zero along a surface which shape depends on parameters δ and χ of the top: the funnel-shape surface in the domain “2”, the bowl-shape surface in the domain “4”, and the cone in the domain “3”; see figures 2 and 3.2–4. Respectively, the instant rotation axis tends asymptotically to the symmetry axis in the domain “2” and to the orthogonal plane in the domain “4” while in the domain “3” the precessing rotation slows down at a constant nutation angle.

In the domain “?” the rotation of the spinning top cannot be considered as a slowly varying precession around the symmetry axis $0\mathbf{e}_3$. Thus we apply to the exact solution (3.9) describing a rotation of the top around the axis $0\mathbf{e}_2$ and consider a perturbation to this solution. It appears unstable but suggests the asymptotical solution “5” with wedge-shape hodograph. The vector of angular velocity ceases in this case by making slow ample waggles around the symmetry axis and narrow waggles in the orthogonal plane. This motion is characteristic for markedly prolate top with sufficiently inclined dipole moment.

In all these cases concerning the askew-polarized spinning top the angular velocity decreases asymptotically to zero by the power law $\Omega \sim 1/\sqrt{\tau_0 t}$.

Another behavior can be revealed by the spinning top with longitudinal polarization. In this

case the reduced Euler equations possess non-zero fixed points and admit an exponential drift of the angular velocity to these points in the characteristic time $\Theta \sim 1/(\tau_0 \Omega_{\parallel}^2 I_{\parallel}^2 / I_{\perp}^2)$ depending on the conserved angular velocity component Ω_{\parallel} along the symmetry axis. Similar behavior may occur in the case of transversal polarization [5]. As a result, the spinning top tends to the final state in which it rotates forever with some residual angular velocity around the dipole moment vector.

On the contrary, the truncated Euler equations predict a power-law spindown for even symmetric particles with the characteristic braking time $T \sim 1/(\tau_0 \Omega_{\perp 0}^2)$ depending on the initial transversal angular velocity $\Omega_{\perp 0}$.

As an experimental test for the correct radiation reaction torque may serve strongly polarized nanoparticles. But even enormous dipole moment 4400 D of the existing slender cellulose nanocrystals [4] is not sufficient to detect the radiation reaction spindown. Indeed, being spun up to GHz they take cosmological period of $\Theta \sim 10^{10}$ years to go to the final state of residual rotation predicted by the reduced Euler equations. Instead, during the much shorter but geological time of $T \sim 10^6$ years one might observe a spindown by the power law which coincides with that predicted by the truncated equations.

A better experimental test to distinguish between two aforementioned frameworks might be a cubic DAST-nanocrystal of size, say $a = 100$ nm, possessing, in theory [12], the giant dipole moment $d = 5.6 \cdot 10^7$ D. We suppose that it can be spun up to the initial angular velocity $\Omega_0 = \pi \cdot 10^{10}$ Hz, as in the experiment [2]. Then such a nanocrystal could serve as a test for choosing between balance equations (2.1) and (2.4a).

Following (2.1), the nanocrystal changes markedly its rotation in the characteristic time $T \sim 1/(\tau_0 \Omega_0^2) \sim 4$ days. Namely, it drifts to its final state of a constant rotation around the dipole vector. Following (2.4a), the slowdown is most intense during the same time and then it continues to stop by the power law $\Omega \sim 1/\sqrt{\tau_0 t}$. The experimental problem in this test is a storage of neutral polarized nanoparticles free or, at least, almost free for few days. For this purpose might serve the currently designing trap for polar particles [16].

References

- [1] Reimann, R., Doderer, M., Hebestrait, E., Diehl, R., Frimmer, M., Windey, D., Tebbenjohanns, F., Novotny, L.: Ghz rotation of an optically trapped nanoparticle in vacuum. *Phys. Rev. Lett* **121**(3), 033602 (2018) <https://doi.org/10.1103/PhysRevLett.121.033602>
- [2] Jin, Y., Yan, J., Rahman, S.J., Li, J., Yu, X., Zhang, J.: 6 GHz hyperfast rotation of an optically levitated nanoparticle in vacuum. *Photon. Res.* **9**(7), 1344–1350 (2021) <https://doi.org/10.1364/PRJ.422975>
- [3] Shanbhag, S., Kotov, N.A.: On the origin of a permanent dipole moment in nanocrystals with a cubic crystal lattice: Effects of truncation, stabilizers, and medium for CdS tetrahedral homologues. *J. Phys. Chem. B* **110**(25), 12211–12217 (2006) <https://doi.org/10.1021/jp0611119>
- [4] Frka-Petesic, B., Jean, B., Heux, L.: First experimental evidence of a giant permanent electric-dipole moment in cellulose nanocrystals. *Europhys. Lett.* **107**(2), 28006 (2014) <https://doi.org/10.1209/0295-5075/107/28006>
- [5] Duviryak, A.: Rotary dynamics of the rigid body electric dipole under the radiation reaction. *Eur. Phys. J. D* **74**(9), 189 (2020) <https://doi.org/10.1140/epjd/e2020-100605-3>
- [6] Duviryak, A.: On the free rotation of a polarized spinning-top as a test of the correct radiation reaction torque. *Eur. J. Phys.* **43**(3), 035203 (2022) <https://doi.org/10.1088/1361-6404/ac578c>
- [7] Landau, L.D., Lifshitz, E.M.: *The Classical Theory of Fields*, 4th edn. – Course of theoretical physics, vol. 2. Butterworth-Heinemann, Oxford (1987)
- [8] Jackson, J.D.: *Classical Electrodynamics*, 3rd edn. Wiley, New York (1999)
- [9] Schott, G.A.: *Electromagnetic Radiation and the Mechanical Reactions Arising from It*. Cambridge University Press, Cambridge (1912)
- [10] Grøn, Ø.: The significance of the Schott energy for energy-momentum conservation of a radiating charge obeying the Lorentz–Abraham–Dirac equation. *Am. J. Phys.* **79**(1), 115–122 (2011) <https://doi.org/10.1119/1.3488985>
- [11] Singal, A.K.: Compatibility of Larmor’s formula with radiation reaction for an accelerated charge. *Found. Phys.* **46**(5), 554–574 (2016) <https://doi.org/10.1007/s10701-015-9978-2>
- [12] Masuhara, H., Nakanishi, H., Sasaki, K.: *Single Organic Nanoparticles*. Springer, Berlin (2003), pp. 387–390
- [13] Bellman, R.: *Stability Theory of Differential Equations*. McGraw-Hill, New York (1953)
- [14] Mitropolsky, Y.A., Nguyen Van Dao: *Applied asymptotic methods in nonlinear oscillations. – Solid Mechanics and Its Applications*, vol. 55. Springer, Dordrecht (1997)
- [15] Häffner, H., Beier, T., Djekić, S., Hermanspahn, N., Kluge, H.-J., Quint, W., Stahl, S., Verdú, J., Valenzuela, T., Werth, G.: Double Penning trap technique for precise g factor determinations in highly charged ions. *Eur. Phys. J. D* **22**(2), 163–182 (2003) <https://doi.org/10.1140/epjd/e2003-00012-2>
- [16] Przybylska, M., Maciejewski, A.J., Yaremko, Y.: Electromagnetic trap for polar particles. *New Journal of Physics* **22**(10), 103047 (2020) <https://doi.org/10.1088/1367-2630/abb913>